Nonlinear Processes in Geophysics, 12, 1003–1009, 2005
SRef-ID: 1607-7946/npg/2005-12-1003
European Geosciences Union


Nonlinear Processes in Geophysics

# Chaotic ray propagation in corrugated layers

**M. Bottiglieri**[1], **S. De Martino**[2], **M. Falanga**[2], **and C. Godano**[1]

[1]Environmental Department, Second University of Naples, via Vivaldi 43, 81100 Caserta and CNISM, Italy
[2]Physics Department, University of Salerno, via S. Allende, 84081 Baronissi Salerno and INFN – Gruppo collegato di Salerno, Italy

Received: 23 June 2004 – Revised: 12 May 2005 – Accepted: 12 July 2005 – Published: 21 November 2005

**Abstract.** The aim of this paper is to study the effects of a corrugated wall on the behaviour of propagating rays. Different types of corrugation are considered, using different distributions of the corrugation heights: white Gaussian, power law, self-affine perturbation. In phase space, a prevalent chaotic behaviour of rays, and the presence of a lot of caustics, are observed. These results entail that the KAM theorem is not fulfilled.

## 1 Introduction

Ray theory has been successfully used in many branches of physics (optics, geophysics and any field where wave propagation is relevant) and it can explain many experimental observations, like travel time curves, wave amplitudes, interference, etc. A very interesting phenomenon, for which ray theory has found application, is the formation of waveguide channels, along which the waves propagate at very long distances. This occurs when the waves propagate without significant diffractive losses, and has been studied for the light radiation in optical fibres (Unger, 1977), short radio waves in atmosphere (Gurevich and Tsedilina, 1975), low frequency sound waves in the ocean (Keller and Papadakis, 1977). Among many factors affecting this behaviour, the most investigated is the presence of regular inhomogeneities along the wave propagation direction. A periodic perturbation of the waveguide has been studied for the ionosphere (Gurevich and Tsedilina, 1975), internal waves in the ocean (Keller and Papadakis, 1977), and seismic wave propagation in the Earth's crust (Keers et al., 1996). Chaotic behaviour inferred from propagation has also been analyzed (Palmer et al., 1988; Tappert et al., 1991; Abdullaev, 1991). Ray theory fails in very heterogeneous media, meaning that when rays cross, a caustic results, i.e. a subdivision of the space in different regions of multipathing, not allowing an easy analytic treatment. Even when waveguides with smooth heterogeneities are considered, a chaotic behaviour can appear (Keers et al., 1997). Similar results can also be obtained by varying the refraction index along the transverse coordinate (Abdullaev, 1991). Another group of strongly chaotic systems, which makes use of ray theory, can be constructed from certain classes of "billiard" problems (Bunimovic, 1979; Sinai, 1970).

Here, we study the behaviour of ray propagation in a waveguide with an irregular interface, attempting to reproduce the wave propagation in real randomly corrugated Earth layers. In particular, we analyze three types of corrugation: a Gaussian white noise, a power law distribution and a self-affine corrugation.

The paper is organized as follows: in Sect. 2 we mention the general features of Hamiltonian chaos; in Sect. 3 we illustrate the general strategy of ray propagation in the waveguide; Sect. 3.1 illustrates the results related to Gaussian white noise, whereas the results for power law distribution and self-affine profiles are shown in Sects. 3.2 and 3.3, respectively. In Sect. 4 we shall draw our conclusions.

## 2 Hamiltonian chaos

Ray propagation in a waveguide is regarded as a Hamiltonian problem with periodic solutions. However, even by perturbing the Hamiltonian with a periodic potential, as is, for example, Abdullaev (1991), chaotic zones in the phase space are obtained. Periodic behaviour in the phase space is easily recognizable in the case of a few degrees of freedom. Namely, we have ellipsoidal shaped trajectories in the two-dimensional case. More generally, the dynamics will evolve on an N-dimensional torus and we shall observe a quasi-periodic behaviour. Note that quasi-periodicity is described by the relation $\boldsymbol{m}\times\boldsymbol{\omega}=0$, where $\boldsymbol{m}$ is a vector of integers (except the trivial vector of components equal to zero) and $\boldsymbol{\omega}$ is the vector of the angular velocities. In this case, if one randomly takes a point in the phase space, its dynamics evolves

*Correspondence to:* C. Godano
(cataldo.godano@unina2.it)

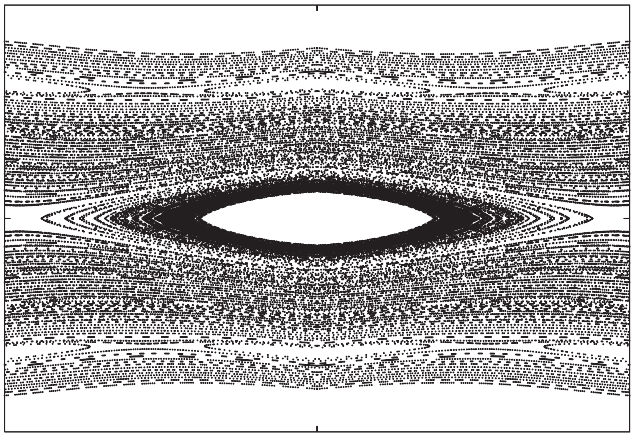

**Fig. 1.** Smoothly perturbed harmonic oscillator map.

on a torus which will completely be filled by the N-frequency oscillations of the system.

### 2.1 KAM theorem

What happens when we perturb the Hamiltonian of an integrable system? Let us consider the following Hamiltonian

$$\mathrm{H}(\boldsymbol{p},\boldsymbol{q}) : \mathrm{H}(\boldsymbol{p},\boldsymbol{q}) = \mathrm{H}_0(\boldsymbol{p},\boldsymbol{q}) + \varepsilon \mathrm{H}_1(\boldsymbol{p},\boldsymbol{q}) \,, \qquad (1)$$

where $\mathrm{H}_0$ is unperturbed and $\mathrm{H}_1$ is the perturbation. We expect that, for small $\varepsilon$, orbits initially approximate those of the integrable system and stay very close to the unperturbed N-tori for some time. However, a given orbit when followed for enough time could ergodically wander anywhere on the energy surface. It should not be surprising that the true situation lies somewhere between the two extremes. Without going into the details of the KAM theorem, we can say that it essentially states that, under very general conditions and for small values of $\varepsilon$, "most" (in the sense of the Lebesgue measure in the phase space) of the unperturbed tori survive. More formally, this means that if we have a torus of the unperturbed system with frequency vector $\boldsymbol{\omega_0}$, there exists a torus of the perturbed system which has a frequency vector $\boldsymbol{\omega(\varepsilon)}=k(\varepsilon)\boldsymbol{\omega_0}$, where $k(\varepsilon)\to 1$ as $\varepsilon\to 0$ (Ott, 1993). As a final observation, we note that the so-called resonant tori (the ones for which $\boldsymbol{m}\times\boldsymbol{\omega_0}=0$) will be destroyed by the perturbation for any $\varepsilon>0$. According to the KAM theorem, for small values of $\varepsilon$, the perturbed system phase space volume (Lebesgue measure) not occupied by the surviving tori is small and approaches zero as $\varepsilon$ approaches zero.

### 2.2 Fractality in phase space

The resonant tori are dense, so we expect that in the proximity of the surviving tori of the perturbed system there will be regions, as small as desiderated, occupied by chaotic orbits, as well as new tori created by perturbation. The set in phase space occupied by surviving perturbed tori is called a fat fractal (Ott, 1993). For completeness, we would like to mention that some Hamiltonian systems show a phase space characterized by chaotic behavior, not because they lack integrability, but because the Hamiltonian has singularities (points in which it is not differentiable). These points arise, for example, in the models of collisions of rigid billiard balls. Notice that a billiard is a two-dimensional planar domain in which a point particle moves with constant velocity, along straight line orbits between specular bounces (angle of incidence = angle of reflection) from the domain boundaries (Ott, 1993; Hilborn, 1994). Some examples of Hamiltonian perturbed systems are the standard map (Ott, 1993), nonturbulent mixing in fluids (Aref, 1984; Chaiken et al., 1986; Feingold et al., 1988), the trajectories of magnetic field lines in plasma (Rosenbluth et al., 1966; Finn, 1975; Hanson and Cary, 1984) and many others. The phase space of a perturbed periodic system is shown in Fig. 1, where a smoothly perturbed harmonic oscillator is presented.

## 3 Ray propagation

In most cases of the quoted literature, including the papers concerning seismic rays, the Hamiltonian system (the ray propagating in a waveguide or an Earth layer) has been periodically perturbed (resonant waveguide). The ray propagation in a resonant waveguide can be investigated analytically or numerically, providing interesting results in the field of Hamiltonian chaos (for a detailed and exhaustive discussion, see Abdullaev, 1992).

For real systems a periodic perturbation could be an oversimplification. A more realistic description of the Earth's structure should include the real topography of the Earth's landscapes. Here we try to reproduce the real Earth structures by means of randomly corrugated interfaces, which should simulate the true topography of the Earth. In order to investigate the influence of a complex corrugation of the waveguide, we perform a numeric parametric study perturbing the Hamiltonian with different noises. Practically, this corresponds to adding an effective potential due to the corrugated interface. Thus, in our simulations, the noise is added to an initially flat interface, which, as a result, will be irregularly corrugated, perturbing the ray motion in a complex way depending on the chosen noise. Notice that the physical dimension of the layer corrugation should be at least equal to the wavelength of the propagated wave, in order to make the scattering possible. The average velocity of the P waves in the Earth's crust is $\approx 3.5\,\mathrm{km}^{-1}$, typical frequencies of seismic waves are in the range 1–30 Hz; this implies that their wavelength is in the range 3.5–120 km. Thus, the largest wavelength have the dimension of a hill, implying that our simulations have the dimensions of a true Earth.

We shall show that, as a final result, the KAM theorem is not fulfilled anymore. Indeed, the tori are generally destroyed, except for some take-off angles or for some amplitudes of the perturbation added to the flat interface.

The simulation has been performed by propagating the ray in a layer with length $l=100$ km and width $h=1$ km. The

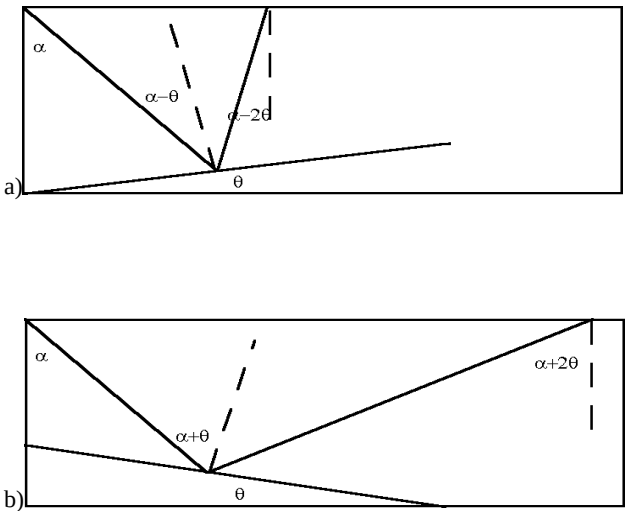


**Fig. 2.** A portion of the lower interface between two successive points at different heights is shown as an example, when **(a)** the reflector is up-going, **(b)** the reflector is down-going. Dotted lines represent the seismic rays propagating in the simulated Earth layer. Dashed lines are perpendicular to the lower and upper interfaces. Proportions are not respected.

upper interface was flat, whereas the bottom interface was corrugated. The source was placed in the upper left corner of the waveguide and the ray propagated according to Snell's law. The distance covered by the ray on the upper interface at each reflection can be evaluated by means of very simple trigonometric manipulations (for a sketch of the geometry, see Fig. 2):

$$\Delta x^{up} = y(n)\tan(\alpha-\theta)\left[1+\frac{\cos\alpha}{\cos(\alpha-2\theta)}\right] \quad (2)$$

$$\Delta x^{dw} = y(n)\tan(\alpha+\theta)\left[1+\frac{\cos\alpha}{\cos(\alpha+2\theta)}\right], \quad (3)$$

where $\alpha$ is the take-off angle of the ray, $\vartheta$ is the inclination angle of the reflector, $y(n)$ is the ordinate of the impact point of the ray on the reflector and $n$ is the index of the propagation step. After each reflection the new take-off angle is:

$$\alpha_n^{up} = \alpha_{n-1} - 2\theta \quad (4)$$

$$\alpha_n^{dw} = \alpha_{n-1} + 2\theta\,. \quad (5)$$

The phase space for each angle is represented by all the coordinate couples $(d,\alpha)$ ($d$ is the horizontal distance covered by the ray expressed in km), for any initial take-off angle $\alpha_0$. The choice of these variables is due to their interest in seismology and to our aim of making our results comparable with those of other authors (Keers et al., 1996, 1997). In order to avoid any dependence on the particular configuration of the corrugated interface, we have generated 200 different profiles for each $\alpha_0$, and the propagation procedure has been repeated for each one of them. Then $\alpha_0$ is increased by 0.1° and the whole process is repeated. We plot the manifold of the phase space for a single given initial condition and the complete phase space, where all the initial conditions are joint in a single representation. The corrugated interface has been created by joining 33 points, equispaced in abscissa, whereas the ordinate value is given by:

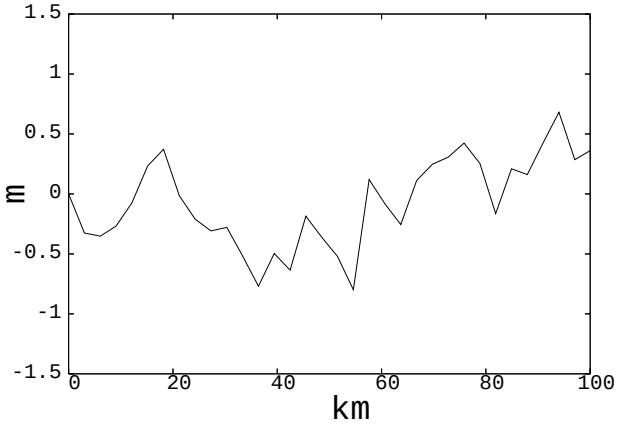


**Fig. 3.** Example of lower interface. Height has a Gaussian white distribution with variance=1.0 km$^2$. Thirty-three points are plotted.

– a random number with zero mean Gaussian distribution and fixed variance;

– a power law distribution;

– a self-affine perturbation.

We chose these perturbations in order to simulate real landscapes in three different cases: random noise with finite variance, random noise with infinite variance, self-affine perturbation, the best simulation of the Earth is topography (Turcotte, 1997; Malamud and Turcotte, 1999).

### 3.1 Gaussian white noise

Our first simulation has been performed by perturbing the lower flat interface with a Gaussian white noise. Many simulations (see an example in Fig. 3) have been made for different values of the variance, in order to understand the ray's propagation. Notice that here the variance of the noise represents the amplitude of the perturbation $\varepsilon$. The scale of the variance has been set equal to $h\times10^{-3}$. This choice derives from a compromise between the significance of the perturbation (lower values do not affect the periodic propagation) and the possibility of a free propagation (higher values trap the ray not allowing a propagation through the layer). In this case, we have noticed that, for small values of variance, the phase space is characterized by the presence of some residues of surviving 1-tori, whereas these disappear more rapidly for large values of variance. Let us comment about each variance value:

– Variance equal to $1.0\times10^{-5}$ km$^2$. We can observe the presence of residual tori in the region of $\alpha$ in the range

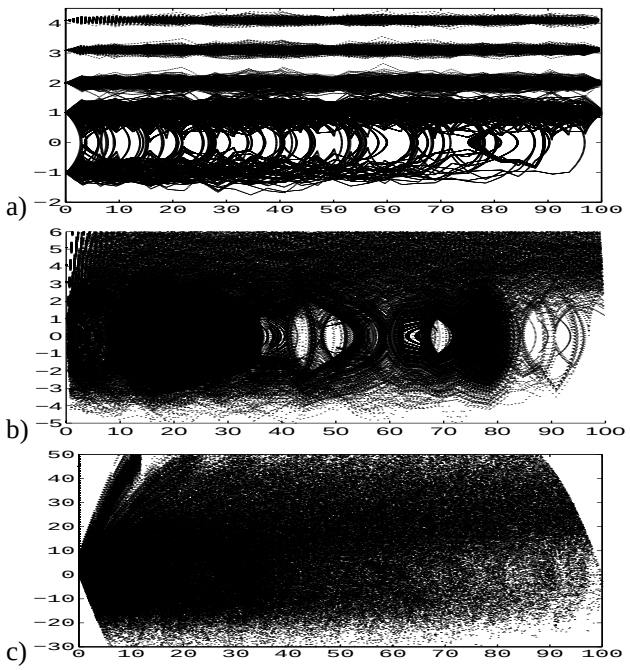


**Fig. 4.** Complete phase space associated with ray propagation in a waveguide characterized by a Gaussian white lower interface. Different variances are shown: **(a)** variance=$1.0\times10^{-5}$ km$^2$, **(b)** variance=$1.0\times10^{-3}$ km$^2$, **(c)** variance=1.0 km$^2$.

$(-1.5°, 1.5°)$ for low values of $\alpha_0$(1.0°, 1.3°). For higher values of $\alpha_0$, we observe a chaotic region, and the expected regions of regularity are represented by horizontal lines.

– Variance equal to $1.0\times10^{-4}$ km$^2$. In this case, we observe a similar behaviour as in the previous one. But here the $\alpha_0$ range, for which we observe a residual toroidal region is increased up to 2.3°.

– Variance equal to $1.0\times10^{-3}$ km$^2$. The residual toroidal zone acquires a fractal structure clearly recognizable at various epicentral distances for different values of $\alpha_0$. The case of $\alpha_0$=2.0° is particularly interesting: by zooming in on the region 15.0 km$<d<$25.0 km and $-1.0°<\alpha<1.0°$, it is possible to see very clearly the fractal behaviour of the phase space. This characteristic is preserved up to $\alpha_0$=4.5°, where the toroidal region is very poorly populated. The whole phase space reveals how chaotic behaviour begins to dominate the dynamics for this value of the variance.

– Variance equal to $1.0\times10^{-2}$ km$^2$. We observe a very similar behaviour as in the previous case, but for higher values of $\alpha_0$, with a less dense toroidal region.

– Variance equal to $1.0\times10^{-1}$ km$^2$. Again, for still higher values of $\alpha_0$ the toroidal regions are less dense.

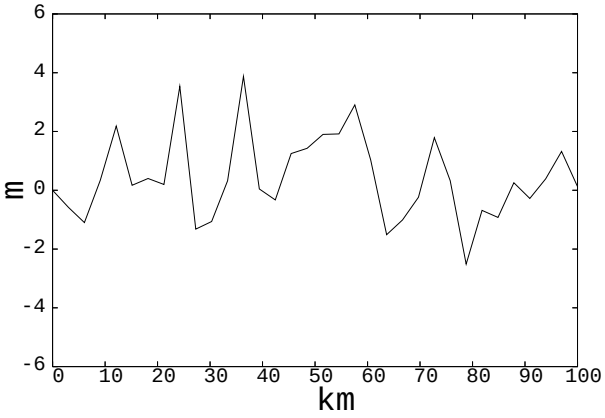


**Fig. 5.** Example of lower interface. Height has a power law distribution with an exponent=1.0. Thirty-three points are plotted.

– Variance equal to 1.0 km$^2$. The trend is confirmed, and the complete phase space is a very dense cloud of points.

Examples are provided in Fig. 4, where we represent the phase space for three different values of the variance. It is clear that the effect of an increasing value of the variance is the disappearence of the region in which the surviving tori are recognizable (compare with Fig. 1). Note that the different scale of the vertical axis is due to a better zooming in on the significant part of the phase space.

### 3.2 Power law distribution

The perturbation of the interface has been obtained, in this case, by adding (or subtracting, with a 50% of probability) to the flat interface, a value randomly chosen among a set of numbers with a power law distribution (see an example in Fig. 5). In this simulation, also, we observe a chaotic behaviour with a central narrow zone, in which it is possible to notice some residual tori. This region tends to disappear as the exponent of the power law distribution increases. As in the previous section, in what follows we analyze the results for the three values of the exponent:

– Exponent equal to 1.0. The manifolds of the phase space for each $\alpha_0$ become less dense as $\alpha_0$ increases and the region of residual tori becomes empty for $\alpha_0>65.0°$. This feature, also observed for the Gaussian white noise, is here clearer. The complete phase space (Fig. 6a) exhibits a behaviour very similar to the Gaussian white noise cases. The central zone is compressed and tends to be confused in the chaotic regions, but a zoom in for $\alpha$ in the range $(-20.0°, 20.0°)$ reveals the existence of residual tori.

– Exponent equal to 1.5. Here the residual toroidal region is still recognizable for $\alpha_0<42.0°$, whereas it completely disappears for the other values. The complete phase space (Fig. 6b) shows a clear residual toroidal zone.

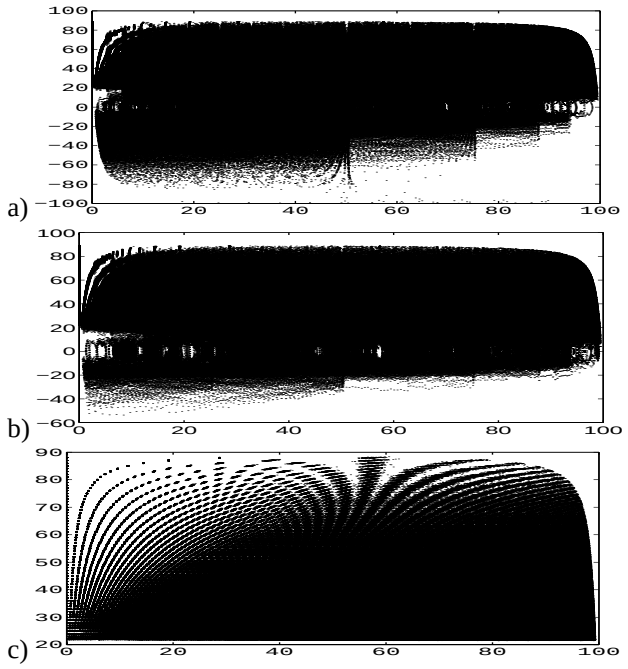


**Fig. 6.** Complete phase space associated with ray propagation in a waveguide characterized by a power law distribution lower interface. Different exponent are shown: **(a)** Exponent=1.0, **(b)** Exponent=1.5, **(c)** Exponent=2.0.

– Exponent equal to 2.0. The phase space is completely chaotic for any $\alpha_0$ and, obviously, we can observe the same feature for the whole phase space (Fig. 6c).

### 3.3 Self-affine perturbation

The last simulation has been performed by using a self-affine corrugated wall: a statistically self-affine fractal is generally nonisotropic, given that the $x$ and $y$ coordinates are scaled differently. For this waveguide, the lower interface has been built by means of the midpoint displacement method (Russ, 1994). This is one of the most straightforward methods to generate a self-affine profile. Starting with the entire length of a linear array, the midpoint is displaced up or down by a random amount. This procedure is repeated for each of the two segments to produce four, and continues down to the individual points. The magnitude of each displacement is reduced as the length of the segment is reduced, so that for a length scale $r_n = \frac{1}{2^n}$, the displacement shall be scaled as

$$r^{2\xi} \tag{6}$$

and the fractal dimension shall be $D_F = 2-\xi$. In other words, the construction starts with a straight (Euclidean) line between two points. Then, the midpoint of the line is displaced by some random amount $\langle z \rangle$, either up or down, with equal probability. This creates a line with two straight segments, and the procedure is repeated for each one of their midpoints. Again, the midpoints of the new segments are displaced by

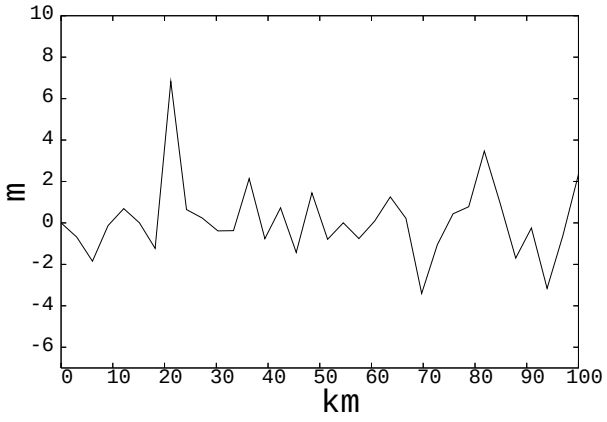


**Fig. 7.** Example of a self-affine profile, building dimension is: $D_F = 1.5$ and $\sigma = h \times 10^{-4}$. Thirty-three points are plotted.

a quantity rescaled according to relation (6) and so on, down to a previously chosen threshold value of the segment length. Generally, $\langle z \rangle$ is obtained by using a Gaussian random number generator with the standard deviation rescaled according to relation (6). The coefficient $\xi$, the Hurst's exponent in the range (0, 1), turns out to control the fractal dimension of the line. For the particular waveguide considered here, we have decided to stop the construction at 5th step, i.e. 31 segments. We underline the fact that we have 33 points, including the profile's initial and final points (see an example in Fig. 7). Once again, we have considered 200 profiles. In our study, we have used $\xi = 0.9, 0.5, 0.1$, which implies $D_F = 1.1, 1.5, 1.9$, respectively. For each fractal dimension, we have used three different scales of the standard deviation $\sigma$, $h \times 10^{-3}$, $h \times 10^{-4}$, $h \times 10^{-5}$. Observing the phase spaces of these simulations, it is clear that the presence of residues of tori is connected to how much the wall is corrugated: as the fractal dimension increases, the residual tori disappear. The dependence of the phase space on the scale of $\sigma$ is similar to the one observed for the Gaussian white noise. Now we discuss the effects of the self-affine interface perturbation on the phase space as $D_F$ and $\sigma$ vary:

– $D_F = 1.1$, $\sigma = h \times 10^{-3}$ . The residual tori are clearly recognizable for $\alpha_0 < 18.6°$, whereas the whole phase space shows a chaotic regime for the other values of $\alpha_0$.

– $D_F = 1.1$, $\sigma = h \times 10^{-4}$. Here the phase space appears more complex, characterized by a fractal structure of the residual tori for lower values of $\alpha_0$. The complete phase space evidences the existence of regular regions (Fig. 8a).

– $D_F = 1.1$, $\sigma = h \times 10^{-5}$. In this case, the residual tori are less dense but still recognizable, and the complete phase space is more regular.

– $D_F = 1.5$, $\sigma = h \times 10^{-3}$. The behaviour of the rays is very similar to the one of the fractal dimension $D_F = 1.1$, except for a lesser density of the points in the phase space.

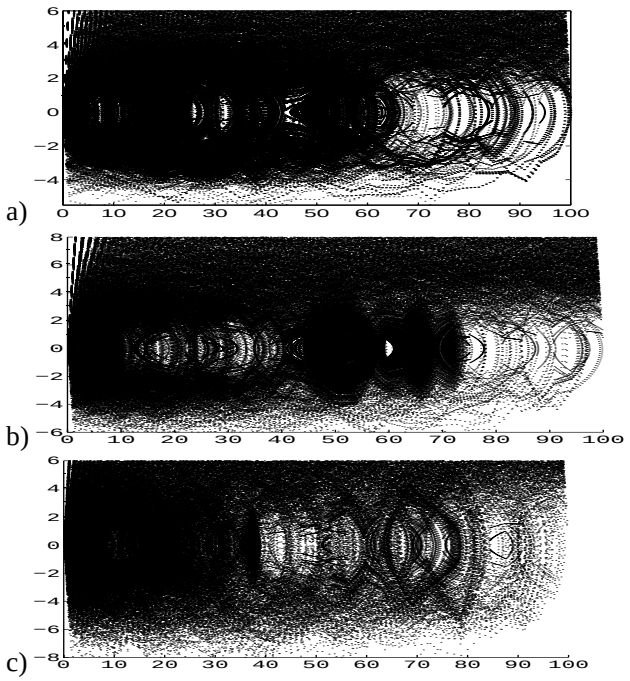


**Fig. 8.** Complete phase space associated with ray propagation in a waveguide characterized by a self-affine lower interface. Different fractal building dimensions and different variances have been showed. **(a)** $D_F$=1.1, $\sigma=h\times10^{-4}$; **(b)** $D_F$=1.5, $\sigma=h\times10^{-4}$; **(c)** $D_F$=1.9, $\sigma=h\times10^{-4}$.

– $D_F$=1.5, $\sigma=h\times10^{-4}$. Once again, the features of the fractal dimension $D_F$=1.1 are repeated with a lesser density of points (Fig. 8b).

– $D_F$=1.5, $\sigma=h\times10^{-5}$. We can observe the same trend as discussed above. Obviously, the same structure is repeated for the fractal dimension $D_F$=1.9 with a lesser density of points (Fig. 8c).

For all the interface perturbations, we estimated the phase space fractal dimension by using the Grassberger and Procaccia algorithm (1983). The values are in the range 1.3−1.7, revealing that the systems' behaviour cannot be considered Hamiltonian: Hamiltonian chaos generates dense, fractal phase spaces, with $D_F$=2.0, which, in fact, are called "fat fractals".

## 4 Conclusions

We attempted to reproduce ray propagation in real Earth layers by simulating such structures by means of corrugated waveguides. In our simulation of the propagation of seismic rays in a layer, we used different kinds of noise: white Gaussian, power law distributed and self-affine noises.

For Gaussian white noise, phase space tends to become a straight line and the residual toroidal zone becomes smaller and smaller as the noise variance increases.

The power law distribution exhibits a more pronounced tendency to the disappearence of the tori as the exponent of the power law distribution increases. The ray propagation on the fractal interface depends on $D_F$ and on the amplitude of the perturbation. If we fix the dimension and make the random number in the building procedure smaller, we can note that the phase space turns again into a straight line; inversely, if the random numbers are larger, the residual tori disappear and all the space becomes chaotic.

In any case, we observe periodic behaviours (straight lines in the phase space) because the rays, for large initial take-off angles, reach the edge of the layer after very few reflections with a poor sampling of the corrugation. For lower initial take-off angles we observe a chaotic regime without any clearly recognizable surviving torus. Most of the tori are distorted into fractal sets, reminiscent of the fractal structure of a phase space arising from a "KAM dynamical system". However, dense, fractal regions are not expected for KAM systems. Thus, we can conclude that a noise structure is a strong perturbation of the Hamiltonian, which makes the KAM theorem not fulfilled any longer.

These results also have very important seismological implications: in chaotic regimes it is impossible to follow the propagation of a single ray, and the different phases of the seismic signal cannot be easily recognized. Moreover, the frequent presence of caustics could explain anomalous amplification of the seismic waves' amplitudes.

*Acknowledgements.* We would like to acknowledge two anonymous reviewers and B. D. Malamud whose criticisms helped us in improving the clearness of the paper.

Edited by: B. D. Malamud
Reviewed by: two referees

## References

Abdullaev, S. S.: Classical chaos and nonlinear dynamics of rays in inhomogeneous media, Chaos, 1, 2, 212–219, 1991.

Abdullaev, S. S.: Chaos and Dynamics of rays in waveguide media, edited by: Zaslavsky, G. M., 185–210, 1992.

Aref, H.: Stirring by Chaotic Advenction, J. Fluid Mech., 143, 1–3, 1984.

Bunimovic, L. A.: On ergodic properties of nowhere dispersing billiards, Comm. Math. Phys., 65, 295–312, 1979.

Chaiken, J., Chevray, R., Tabor, M., and Tan, Q. M.: Experimental Study of Lagrangian Turbolance in Stokes Flow, Proc. Roy. Soc. (Lond.) A, 408, 165–174, 1986.

Chin, B. H. and Aki, K.: Simultaneous study of the source, path and site effects on strong ground motion during the 1989 Loma Prieta earthquake: a preliminary result on pervasive non-linear site effects, Bull. Seism. Soc. Am., 81, 1859–1884, 1991.

Darragh, R. B. and Shakal, A. F.: The site response of two rock and soil station pairs to strong and weak ground motion, Bull. Seism. Soc. Am., 81, 1885–1899, 1991.

Feingold, M., Kadanoff, L. P. and Piro, O.: Passive Scalars Three-Dimensional Volume Preserving Maps, and Chaos, J. Stat. Phys., 50, 529–565, 1988.

Finn, J. M.: The Destruction of Magnetic Surfaces in Tokamaks by Current Perturbations, Nucl. Fusion, 15, 845–852, 1975.

Grassberger, P. and Procaccia, I.: Measuring Strangeness of Strange Attractors, Physica D, 9, 189—208, 1983.

Gurevich, A. I. and Tsedilina, E. E.: Long Distance Propagation of HF Radio Waves, Springer-Verlag, Berlin, 1975.

Hanson, J. D. and Cary, J. R.: Elimination of Stochasticity in Stellerators, Phys. Fluids, 27, 767–769, 1984.

Hilborn, R. C.: Chaos and nonlinear Dynamics, Oxford University Press, 1994.

Keller, J. B. and Papadakis, J. S.: Wave Propagationand Underwater Acoustics, Springer-Verlag, Berlin, 1977.

Keers, H., Nolet, G. and Dahlen, F. A.: Ray theoretical analysis of Lg, Bull. Seism. Soc. Am., 86, 726–736, 1996.

Keers, H., Dahlen, F. A., and Nolet, G.: Chaotic ray behaviour in regional seismology, Geophys. J. Int., 131, 361–380, 1997.

Malamud, B. D. and Turcotte, D. L.: Self-Affine Time Series: I. Generation and Analayses, Adv. Geophys., 40, 1–90, 1999.

Ott, E.: Chaos in dynamical system, Cambridge University Press, 1993.

Palmer, D., R., Brown, M. G., Tappert, F. D., and Bezdek, H. F.: Classical chaos in non separable wave propagation problems, Geophys. Rev. Lett., 15, 569–572, 1988.

Rosenbluth, M. N., Sagdeev, R. Z.,Taylor, J. B., and Zaslavski, G. M.: Destruction Magnetic Surfaces by Magnetic Field Irregularities, Nuc. Fusion, 6, 297–303, 1966.

Russ, J.: Fractal Surfaces, Plenum Press, New York, 1994.

Sinai, Y.: Dynamical system with elastic reflections, Ergodic properties dispersing billiards, Russ. Math. Surv., 25, 137–189, 1970.

Tappert, F. D., Brown, M. G.. and Goni, G.: Weak chaos in an area-preserving mapping for sound ray propagation, Phys. Lett. A, 153, 181–185, 1991.

Turcotte, D.: Fractals and Chaos in Geology and Geophysics, 2nd edition, Cambridge, New York, Cambridge University Press, 1997.

Unger, H. G.: Planar Optical Waveguides and Fibres, Oxford University Press, London, 1977.